ACS APPLIED MATERIALS & INTERFACES

www.acsami.org Research Article

Self-Assembled DNA−Protein Hybrid Nanospheres: Biocompatible Nano-Drug-Carriers for Targeted Cancer Therapy

Dayoung Lee,[⊥] Seungki Baek,[⊥] Young-Youb Kim, Yongbin Bang, Han Na Jung, Hyung-Jun Im,* and Yoon-Kyu Song*

Cite This: https://doi.org/10.1021/acsami.2c10397 Read Online

ACCESS | Metrics & More | Article Recommendations | Supporting Information

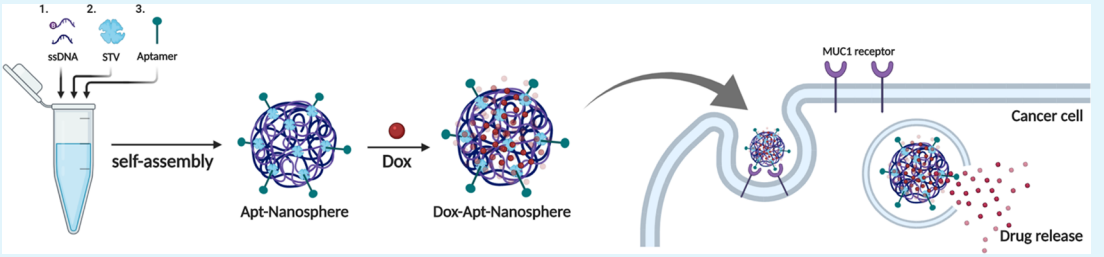

ABSTRACT: We developed hybrid nanospheres comprised of two of the most important biomolecules in nature, DNA and proteins, which have excellent biocompatibility, high drug payload capacity, *in vivo* imaging ability, and *in vitro*/*in vivo* cancer targeting capability. The synthesis can be done in a facile one-pot assembly system that includes three steps: step-growth polymerization of two DNA oligomers, addition of streptavidin to assemble spherical hybrid nanostructures, and functionalization of hybrid nanospheres with biotinylated aptamers. To test the feasibility of cancer targeting and drug-loading capacity of the hybrid nanospheres, MUC1-specific aptamers (MA3) were conjugated to nanosphere surfaces (apt-nanospheres), and doxorubicin (Dox) was loaded into nanospheres by DNA intercalation. The successful construction of nanospheres and apt-nanospheres was confirmed by agarose gel electrophoresis and dynamic light scattering (DLS). Their uniform spherical morphology was confirmed by transmission electron microscopy (TEM). Fluorescence spectra of nanospheres demonstrated high Dox-loading capability and slow-release characteristics. *In vitro* MUC1-specific binding of the apt-nanospheres was confirmed by flow cytometry and confocal microscopy. Dox-loaded apt-nanospheres significantly increased cytotoxicity of the MUC1-positive cancer cells due to aptamer-mediated selective internalization, as shown via cell viability assays. Apt-nanospheres could also be imaged *in vivo* through the synthesis of hybrid nanospheres using fluorescent dye-conjugated DNA strands. Finally, *in vivo* specific targeting ability of apt-nanospheres was confirmed in a MUC1-positive 4T1 tumor-bearing mouse model, whereas apt-nanospheres did not cause any sign of systemic toxicity in normal mice. Taken together, our self-assembled DNA−streptavidin hybrid nanospheres show promise as a biocompatible cancer targeting material for contemporary nanomedical technology.

KEYWORDS: *DNA nanostructures, self-assembly, DNA−protein hybrid, targeted drug delivery, cancer therapy*

INTRODUCTION

Nanotherapeutics have tremendous potential in a wide range of cancer treatment applications, including the enhancement of chemotherapeutic agent delivery, radiation therapy, or immunotherapy effects.[1−3] Recently, explosive advances in nanotechnology have enabled nanotherapeutics to make great progress, particularly in the area of drug delivery.[4,5] These include cancer-specific drug delivery and controlled release of drug cargo, both of which increased therapeutic efficacy against cancers.[6,7] Despite success in drug delivery using nanotechnology, the clinical translation of nanomedicine has been impeded by the systemic toxicity of conventional nanomaterials.[8] Therefore, there has been a consistent demand for development of biocompatible nano-drug-carriers,[9] many of which are based on materials including polymers,[10] inorganic compounds,[11] liposomes,[12] hydrogels,[13,14] dendrimers,[15] proteins,[16] and DNA.[17,18] Among the biocompatible materials, there is a growing interest in DNA and proteins due to their exceptional biocompatibility, programmability, and biofunctionality.[19,20]

Research into the coassembly of DNA and proteins to create hybrid nanostructures is proliferating due to their unique advantages and biocompatibility.[21,22] DNA has the unprecedented precision to build varying nanostructures compared to other types of nanomaterials,[23] while proteins have a myriad of

Received: June 11, 2022
Accepted: August 1, 2022

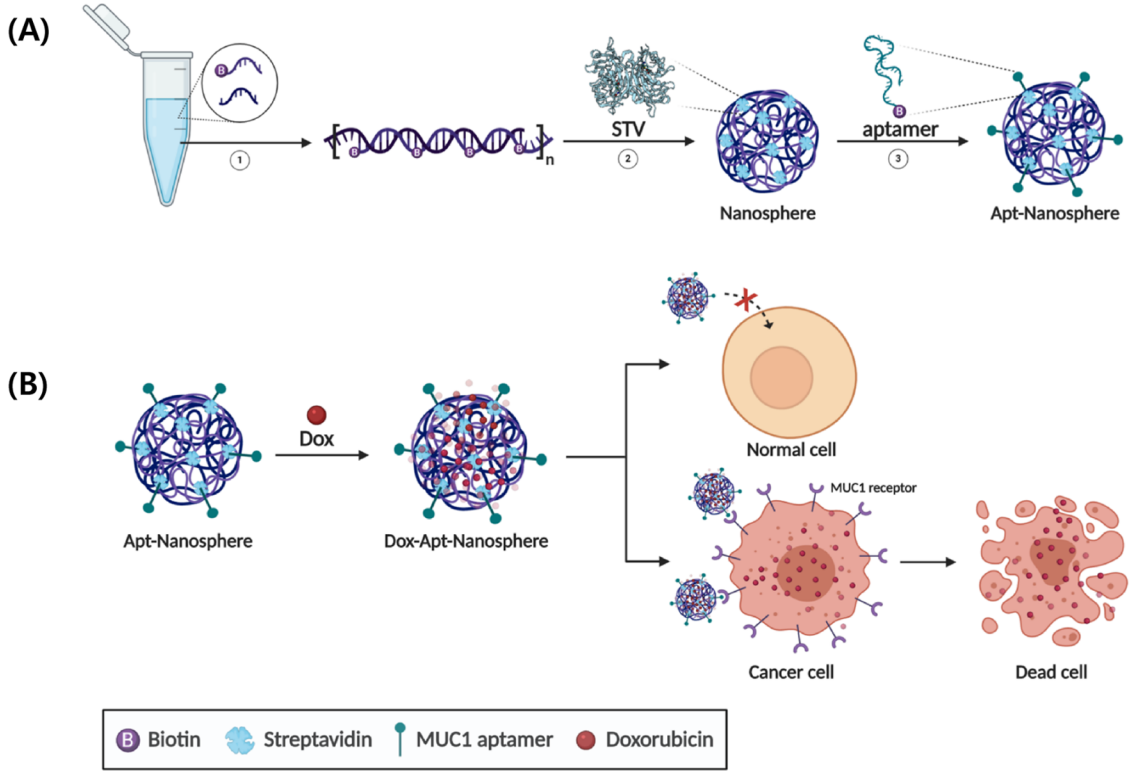

Figure 1. Schematic illustration of (A) three steps of aptamer-conjugated hybrid nanosphere self-assembly (1—step-growth polymerization of DNA oligomers, 2—hybrid nanosphere formation via biotin−streptavidin bioconjugation, and 3—aptamer functionalization into hybrid nanosphere) and (B) its cancer cell-specific intracellular uptake as a targeted drug-carrier.

Table 1. DNA Oligonucleotide Sequences for the Assembly of Apt-Nanospheres

oligomers	sequences (5′ − 3′)
M1	ACGGCTGCGCGACGTAGGTACGGCAACTCGCGGCTATGCA
M1-FAM	[FAM]ACGGCTGCGCGACGTAGGTACGGCAACTCGCGGCTATGCA
M1-Cy5.5	[Cyanine5.5]ACGGCTGCGCGACGTAGGTACGGCAACTCGCGGCTATGCA
M2	[BiotinTEG]TACCTACGTCGCGCAGCCGTTGCATAGCCGCGAGTTGCCG
MA3 (aptamer)	[BiotinTEG] AACCGCCCAAATCCCTAAGAGTCGGACTGCAACCTATGCTATCGTTGATGTCTGTCCAAGCAACACAGACACACTACACACGCACA

known specific biological functions. Therefore, DNA−protein nanostructures have the advantage that they can use DNA as a structural scaffold to generate accurately predicted nanostructures, and proteins can be precisely labeled to perform a variety of functions, synergizing as novel hybrid nanomaterials with functions not possible from an individual biomolecule.[24,25]

Here, we introduce self-assembled DNA−streptavidin hybrid nanospheres that can be easily loaded with chemotherapeutic agents and functionalized to have targeting molecules with versatility. The nanospheres have three reaction stages in the one-pot self-assembly system as shown in Figure 1A. First, biotinylated single-stranded DNA (M2) and half-complementary single-stranded DNA (M1) form a half double-stranded DNA (dsDNA) complex by step-growth polymerization.[26] Subsequently, this dsDNA chain and streptavidin are combined to form hybrid nanospheres via biotin−streptavidin conjugation.[27] Extra streptavidin binding sites allow for further precise functionalization using other biotinylated functional materials (e.g., aptamer, targeting peptide, etc.). Note that streptavidin is a tetrameric protein, allowing the binding of four biotin molecules.[28] The assembly process did not undergo any post-synthetic purification process; thus, we were able to collect nanospheres with sufficient concentrations. In this study, we show the feasibility of precise functionalization using the transmembrane glycoprotein Mucin 1 (MUC1)-specific biotinylated aptamers (MA3) (Figure 1B). Furthermore, nanospheres could be easily loaded with doxorubicin (Dox), a commonly used cytotoxic chemotherapeutic agent, and these loaded nanospheres (Dox-nanospheres) showed a sustained drug release. The aptamer-functionalized and Dox-loaded nanosphere (Dox-apt-nanosphere) exhibited highly selective uptake into MUC1-positive cancer cell lines through a receptor-mediated endocytosis mechanism. In addition, our hybrid nanosphere could be imaged *in vivo* using fluorescent dye-modified M1 and revealed specific *in vivo* targeting of MUC1-positive 4T1 tumor-bearing cells in mouse models. Our self-assembled DNA−streptavidin hybrid nanosphere could be a promising cancer targeted nanoplatform based on their biocompatibility, facile one-pot synthesis, and precise modularity for *in vivo* imaging and cancer targeting.

RESULTS AND DISCUSSION

Self-Assembly of Nanospheres and Aptamer-Conjugated Nanospheres. Nanospheres are synthesized via a

https://doi.org/10.1021/acsami.2c10397
ACS Appl. Mater. Interfaces XXXX, XXX, XXX−XXX

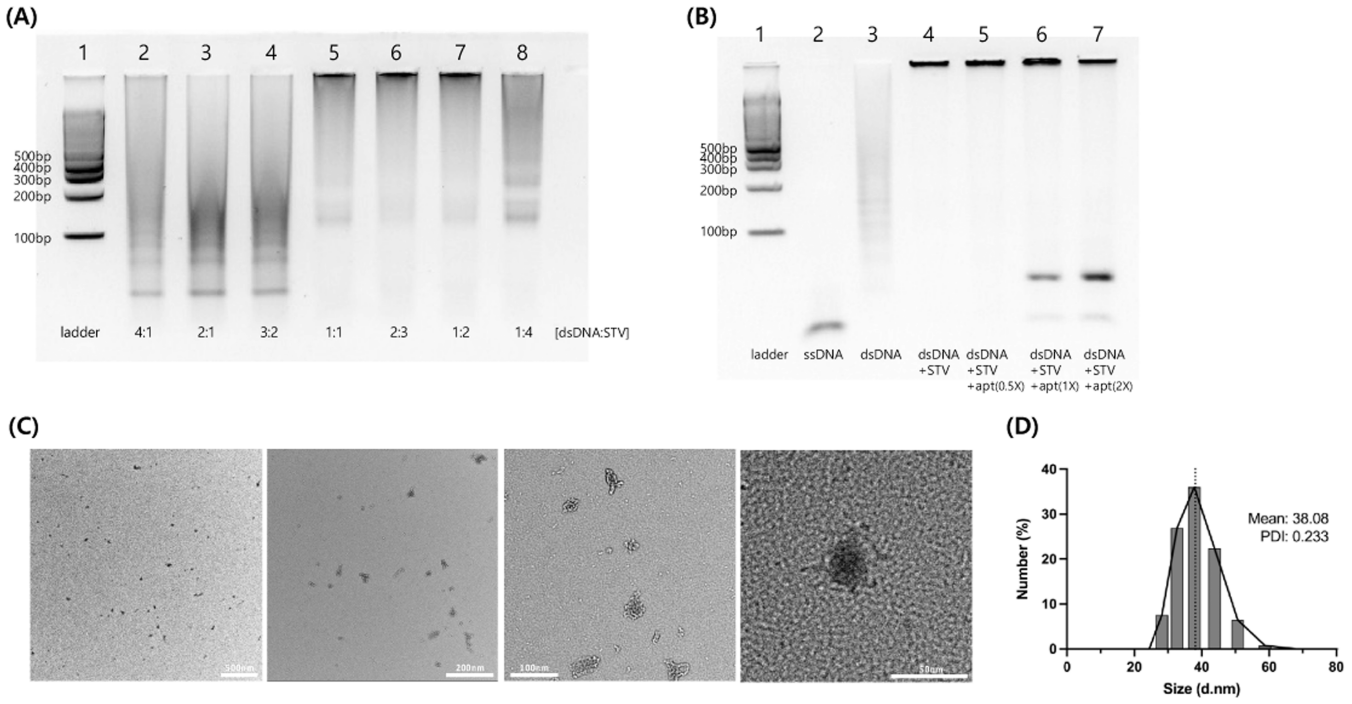

Figure 2. Self-assembled nanosphere characterization. (A) Characterization of the self-assembly of nanospheres by agarose gel electrophoresis. Different ratios of dsDNA and streptavidin were mixed ([dsDNA]:[STV] = 4:1, 2:1, 3:2, 1:1, 2:3, 1:2, 1:4) for 24 h, followed by 3% agarose gel electrophoresis in TBE buffer. (B) Characterization of the self-assembly of nanospheres and aptamer-modified nanospheres by agarose gel electrophoresis. Lanes 1−4 correspond to a 100 base pair ladder, ssDNA (M1), dsDNA (M1 + M2), and nanospheres (M1 + M2 + STV). Lanes 5−7 correspond to different ratios of nanospheres to aptamers corresponding to 2:1, 1:1, and 1:2 from left to right. The samples were synthesized in 20 μM and diluted to 1 μM in 1× phosphate-buffered saline (PBS) before use. (C) Transmission election microscopy (TEM) images characterizing the morphology of nanospheres. (D) Size distribution analyses of nanospheres ([dsDNA]:[STV] = 1:1) by dynamic light scattering (DLS) (n = 10).

one-pot self-assembly process using preprogrammed DNA oligonucleotide sequences, the step-growth hybridization, and the biotin−streptavidin conjugate system, as illustrated in Figure 1A. The two preprogrammed DNA sequences (M1 and M2) used were obtained from a previous study.[29] M1 and M2 have half-complementary sequences specific to each other (all DNA sequences are listed in Table 1) and become a long dsDNA chain through a step-growth polymerization reaction. According to step-growth polymerization kinetics,[30] the average degree of polymerization is determined thermodynamically by the monomer,[31] and thus 40 bp DNA monomers were used at a constant concentration in all experiments. In addition, by simply incorporating streptavidin into an extended double strand DNA chain, the two are combined by molecular recognition of the 5′-biotin-modified DNA oligomer (M2) and streptavidin, integrating into a larger-scale self-assembled supramolecular structure—the nanosphere (detailed procedure in Supporting Information S3). To understand the self-assembly behaviors of these nanospheres, we investigated their assembly using agarose gel electrophoresis (detailed procedure in Supporting Information S4). In addition, we imaged them with transmission electron microscopy (TEM) to better understand the observed structural motifs. By varying the concentrations of streptavidin and dsDNA chain, we identified the most effective nanosphere synthesis ratio. As shown in Figure 2A, when the concentration of dsDNA is higher than that of streptavidin (lanes 2−4), the bands observed were shorter than 200 bp, indicating the unsuccessful formation of hybrid nanospheres. In fact, we often found chain-like structures rather than spherical structures as shown in Figure S1, and we concluded that this is not an appropriate ratio for synthesizing nanospheres as they do not form a uniform spherical structure. Also, when the concentration of streptavidin reaches that of dsDNA (lanes 5−7), the main band was seen near wells, indicating that large-sized new hybrid nanostructures could be constructed in this ratio range. Consistent with gel electrophoresis, it was confirmed that a new type of spherical nanostructure was synthesized in Figure S1. Among this new type of nanostructure, the synthesized nanostructure was with a fixed 1:1 ratio of dsDNA to streptavidin, and we named it nanosphere. Figure 2C confirms the successful self-assembly of nanospheres. Dynamic light scattering (DLS) analyses were also carried out to understand the self-assembly behaviors of nanospheres (Figure 2D). However, when the [dsDNA]:[STV] ratio exceeds 1:4, the nanosphere band near the well cannot be seen. Similarly, in Figure S1, when streptavidin was added up to four times that of dsDNA, the structure changed significantly.

Furthermore, to make nanospheres a targeted drug-carrier for cancer cells, we used aptamers as target ligands.[32] Like antibodies, aptamers are single-stranded nucleic acid oligomers that can, with great specificity, uniquely bind to target proteins that are overly expressed in cancer cells.[33] Here, we have selected MA3, an aptamer that specifically binds to the MUC1 membrane protein, well known for its over-expression in most adenocarcinomas,[34] as illustrated in a previous study by Hu et al.[35] The MA3 aptamer selectively binds toward target MUC1-positive cells such as the T-47D[36] and 4T1 cell lines[37] whereas MUC1-negative cells, such as the HEK293 (human embryonic kidney) cell line,[38] have no significant reaction. In addition,

https://doi.org/10.1021/acsami.2c10397
ACS Appl. Mater. Interfaces XXXX, XXX, XXX−XXX

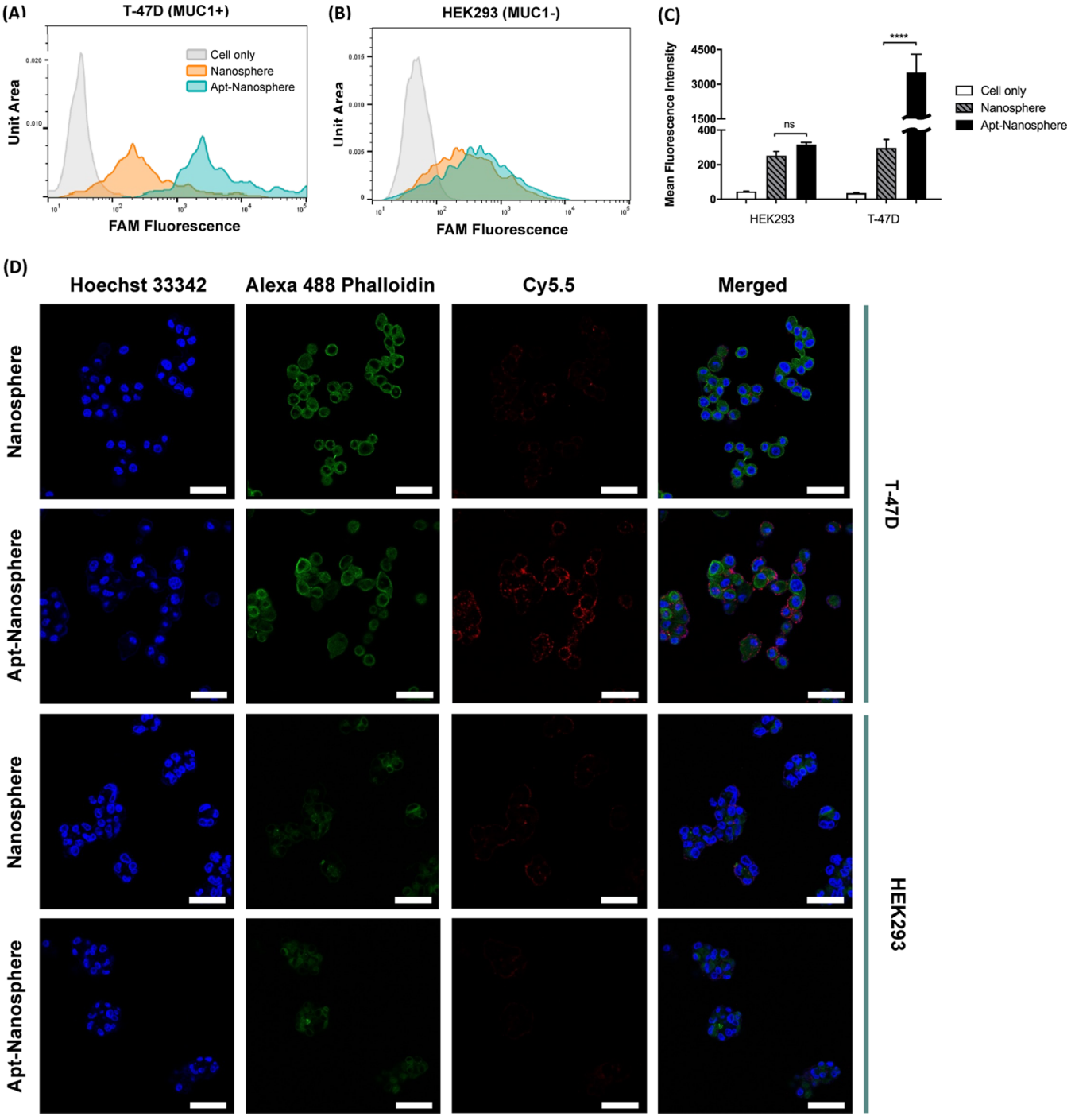

Figure 3. (A, B) Flow cytometry of nontarget HEK293 cells and target T-47D cells treated with nanospheres and apt-nanospheres. (C) Mean fluorescence intensities (MFIs) of T-47D and HEK293 cells were analyzed by Flowjo software after incubation with FAM-labeled nanospheres and apt-nanospheres for 30 min in binding buffer. Data expressed as mean ± SEM (n = 3) (**** indicates significance with $p < 0.0001$ and ns indicates $P > 0.05$). (D) Comparison of cellular internalization of Cy5.5-labeled nanospheres and apt-nanospheres in target T-47D cells and nontarget HEK293 cells (nuclei stained with Hoechst 33342 dye (blue) and cytoskeleton stained with Alexa 488 phalloidin dye (green), scale bar = 50 nm).

biotinylating the aptamers made it easier and faster for them to attach to the scaffold and functionalize nanosphere structures. By simply mixing biotinylated aptamers with nanospheres in solution, we could observe their integration into nanospheres as shown in Figure 2B (lanes 5−7).

We hypothesized that the aptamers were attached to the remaining biotin-binding sites on streptavidin, exposed at the surface of the nanosphere. We performed gel electrophoresis by adjusting the ratio of aptamers to nanospheres (Figure 2B). When we applied a 2:1 ratio of nanospheres to aptamers (lane 5), there was no significant difference from nanospheres (lane 4). Interestingly, the excess aptamers were observed if biotinylated aptamers were added in excess of a 2:1 ratio (lanes 6 and 7). We assumed that this would explain the number of remaining binding sites to which the aptamer could attach. Thus, to better synthesize apt-nanospheres as designed in Figure 1A, we utilized nanospheres with an aptamer of 0.5× in all subsequent experiments to avoid the possibility of the

https://doi.org/10.1021/acsami.2c10397
ACS Appl. Mater. Interfaces XXXX, XXX, XXX−XXX

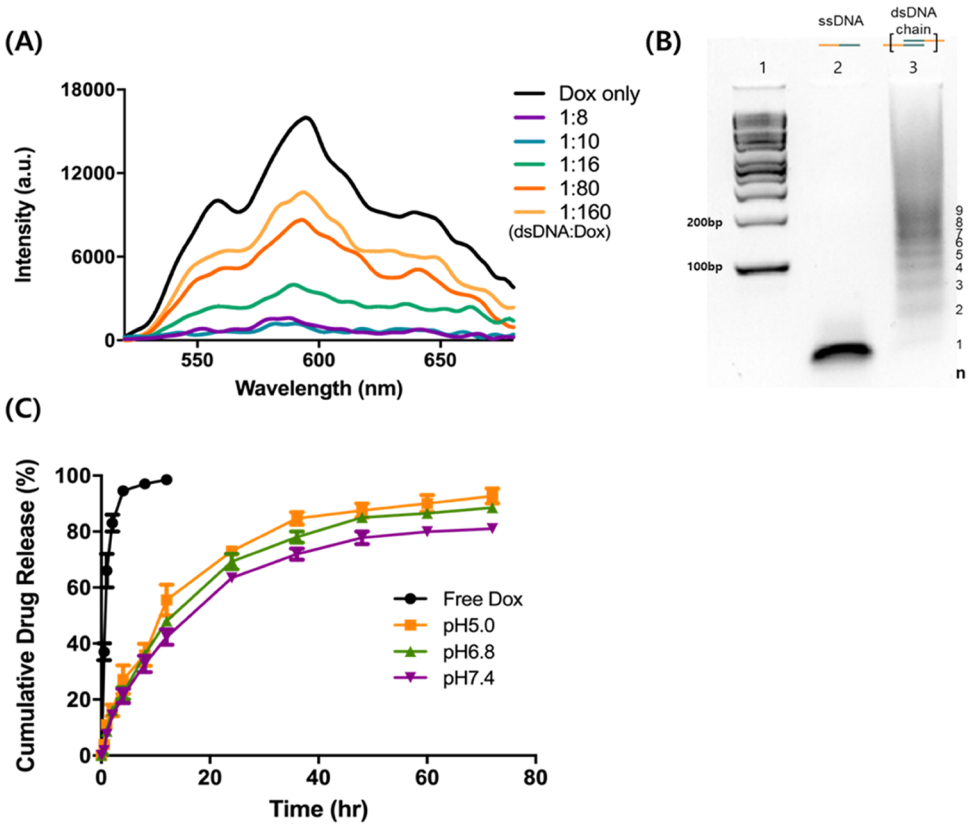

Figure 4. Characterization of the high drug payload capacity of nanospheres. (A) Fluorescence spectra of doxorubicin (Dox) with increasing concentrations of dsDNA to Dox (from top to bottom). (B) 3% Agarose gel electrophoresis in 1× TBE buffer. Lanes 1−3: 100 bp ladder, ssDNA, and dsDNA, respectively. (C) Cumulative drug release profiles: free Dox and nanosphere-Dox in PBS buffers at various pH values. Data expressed as mean ± standard error of the mean (SEM) (n = 3).

blocking effect by excess free aptamers when apt-nanospheres enter the cell.

Our streptavidin−biotin based synthesis and functionalization of hybrid nanospheres have several advantages. First, due to the high affinity of the streptavidin−biotin interaction, it also offers the possibility of structural design, resistance to tumor microenvironments, and stability in denaturing agents among other benefits. Also, the functionalization could be executed without the need for complicated chemical modifications. Furthermore, the optimal ratios of dsDNA to STV and nanosphere to aptamer could be easily identified, and therefore we were able to synthesize uniform hybrid nanospheres with a targeting moiety.

Morphological Analyses of Nanospheres. To understand the morphological features of self-assembled nanospheres, transmission electron microscopy (TEM) and confocal laser scanning microscopy (CLSM) were employed as shown in Figure 2C (detailed procedures in Supporting Information S5) and Figure S2. As expected, nanospheres with a spherical structure are easily detected in Figure 2C at various magnifications using TEM. Figure S2 is a CLSM image of dye-modified hybrid nanospheres, illustrating that FAM-labeled nanospheres can also be used for imaging. FAM-labeled nanospheres were synthesized using M1-FAM, M2, and streptavidin in the same manner as the hybrid nanosphere synthesis described in Supporting Information S3.

Surface Charge Characterization of Nanospheres and Aptamer-Conjugated Nanospheres. When synthesizing drug delivery carriers, their surface charge and surface area are both highly correlated to cellular uptake.[39] Note that nano-drug-carriers of 50−200 nm can passively accumulate in tumor sites via the enhanced permeability and retention (EPR) effect.[40] Moreover, a negative zeta (ζ) potential can affect the pharmacokinetic properties by avoiding random uptake through electrostatic interactions with negatively charged cellular membranes, thus exhibiting excellent serum stability and promoting tumor targeting efficiency.[39] Based on this, we aimed to design highly effective nanocarriers by considering their size and ζ-potential.[41] As shown in Figure S3, ζ-potential measurements identify that negatively charged DNA and streptavidin aggregate to form a hybrid nanosphere, showing a near-zero ζ-potential, which can lead to a steric stabilization of the agglomerate nanosphere in an aqueous suspension. We reasoned that streptavidin could mainly locate on the aggregated dsDNA surface when we introduce streptavidin to dsDNA chains. Therefore, the ζ-potential of the nanosphere is more similar to that of streptavidin than that of dsDNA. The ζ-potential becomes a negative value when the surface of the nanospheres is decorated by introducing an aptamer and loading doxorubicin (Dox).

Furthermore, the nanospheres' ζ-potential value slightly increased when triggered by an acidic extracellular microenvironment (pH 5.0). This change seems to be related to the pH-dependent Dox release, as shown in Figure 4C.

Selective Binding Ability and Cellular Uptake of Apt-Nanospheres. Flow cytometry analyses were performed to investigate the feasibility of aptamers functionalized on nanospheres (detailed procedures in Supporting Information

https://doi.org/10.1021/acsami.2c10397
ACS Appl. Mater. Interfaces XXXX, XXX, XXX−XXX

S9). Figure 1B illustrates the selective binding of hybrid nanospheres functionalized with MA3 aptamers to MUC1 on overexpressed cells through a receptor-mediated endocytosis mechanism,[42] as described by a previous study.[35] FAM-labeled hybrid nanospheres were used to verify the selective binding ability (images of the probe in Figure S2). Both target T-47D cells (A) and nontarget HEK293 cells (B) were independently incubated with nanospheres and apt-nanospheres (1 μM) in binding buffer at 37 °C for 30 min as shown in Figure 3A,B. After 30 min of incubation, only T-47D cells (Figure 3A) showed binding capabilities, as evidenced by the considerable shift in the fluorescence signal compared to that of HEK293 cells (Figure 3B), demonstrating that apt-nanospheres selectively recognize cancer cells. Furthermore, aptamers must function in physiological conditions; thus, the selective recognition ability of apt-nanospheres was investigated in cell culture media, Dulbecco's modified Eagle's medium (DMEM), and binding buffer as shown in Figure S8. We also investigated the binding affinity by varying the number of aptamers and nanospheres. As shown in Figure S8, a 1:2 ratio of aptamers to nanospheres showed the most selective binding. While we could see that aptamer selectivity was slightly lower in cell culture media than in binding buffer, the selectivity was shown almost the same and both were equally effective at a 1:2 aptamer−nanosphere ratio.

Furthermore, cellular internalization is one of the key points of delivering chemotherapeutic agents into target cells to effectively induce cell death. We investigated specific cellular uptake properties of apt-nanospheres in cancer cells (T-47D) by intracellular fluorescence imaging, as shown in Figure 3D (detailed procedures in Supporting Information S10). FAM-labeled nanospheres (100 nM) were used to image the cellular internalization. According to the data, the nanospheres entered neither MUC1-positive nor MUC1-negative cells to a high degree. However, there was a slight uptake of apt-nanospheres into MUC1-negative HEK293 cells, but MUC1-positive T-47D demonstrated significant anchoring of apt-nanospheres to the surface of and uptake into the cell.

Doxorubicin Encapsulation and Sustained Release of Nanospheres. Here, we programmed nanospheres with anticancer capabilities by loading doxorubicin (Dox), a conventional cancer therapy drug. Dox can be intercalated within "GC" or "CG" sequences of DNA due to the presence of aromatic rings.[43] Figure 4A verifies hybrid nanospheres' Dox-loading capabilities and their large drug payloads. To estimate the amount of Dox intercalated into hybrid nanospheres, we incubated a constant concentration of Dox (4 μM) with different concentrations of dsDNA for 6 h at room temperature, as illustrated in Figure 1A (detailed procedure in Supporting Information S6) and explored the loaded-Dox florescence emission spectra (λ_{Ex} = 493 nm, λ_{Em} = 570 nm). In comparison with the emission of free Dox, the fluorescence signal was significantly quenched when dsDNA was incorporated, as shown in Figure 4A. We observed that the higher the concentration of dsDNA added, the larger the decrease in fluorescence intensity. When the concentration ratio of dsDNA to Dox was 1:10, the fluorescence signal was quenched by 94% compared to the fluorescence of free Dox in PBS. However, when the ratio of dsDNA to Dox was 1:8, we observed that there was almost no difference in fluorescence intensity. We therefore quantified that each unit of dsDNA can intercalate ∼10 Dox molecules. In addition, to determine how many ssDNA oligomers comprised each chain, we performed 3% agarose gel electrophoresis to estimate, as shown in Figure 4B. We reasoned that about mostly 7−9 ssDNA oligomers were polymerized to form dsDNA chains that assemble to form a hybrid nanosphere, revealing the possibility that a large amount of drugs could be carried in a single nanosphere.

Sustained drug release at specific sites is clinically important for cancer treatment, increasing therapeutic efficiency and decreasing toxicity.[44] Recognizing the potential benefits of high drug payload of nanospheres, we designed an experiment to assess the drug release behavior of Dox-loaded nanospheres (Dox-nanosphere). The releasing profile of Dox and Dox-nanospheres was investigated in PBS at varying pH values (pH 5.0, 6.8, 7.4) as shown in Figure 4C (detailed procedure in Supporting Information S7). In our initial round of experiments, we first observed the cumulative drug release profile. As shown by the black line in Figure 4, the fluorescence intensity rapidly increases, indicating a burst release of Dox. The drug release profile of Dox in nanospheres was subsequently examined, and we found that it has a characteristic of sustained release via diffusion, which is effective for treating tumors without adverse side effects.[45] As shown in Figure 4C, we verified that over 81.1% of Dox was released from the nanosphere in PBS at pH 7.4. We expected the amount of drug release to change with pH, that lower pH conditions would result in higher percentages of Dox released, as evidenced by previous studies.[46,47] This indicates that in cancer cell lysosomal pH conditions, the hybrid nanosphere can deliver Dox more effectively. At pH 5.0, the cumulative drug release gradually increases, and 92.7% of Dox is released over 72 h. It is noteworthy that the difference in the amount of release of Dox by pH change was not very large, which indicates the release mechanism is probably closer to diffusion than pH-triggered release due to the strong binding from a 40 bp complementary sequence. However, stability in biological conditions must be considered to be suitable for localized and sustained release of Dox-apt-nanospheres.

Nuclease and Serum Stability of Nanospheres. DNA nanostructures are widely used in the biomedical field. However, their short half-life due to rapid degradation by nucleases is a core limitation, hindering their applicability. The nanosphere, a hybrid structure of DNA and streptavidin, is designed to solve the stability issues of DNA nanostructures. To assess the stability of hybrid nanospheres under a nuclease treatment,[48] dsDNA chain and nanospheres were incubated with DNase I at 37 °C for different time durations (procedure detailed in Supporting Information S8). As shown in Figure S4A, nanosphere structures remained intact even after treatment with DNase I (0.05 U/μL) for 1 h, while dsDNA chains were digested as shown in Figure S4B. Only after further incubation for more than 120 min did the nanosphere structures slowly degrade. Consequently, the nanospheres showed higher stability in comparison with dsDNA chains. In addition, Figure S4C,D reveals that both dsDNA chains and nanospheres were stable in cell culture media (10% fetal bovine serum (FBS), 1% PenStrep, DMEM) at 37 °C for 240 min. Finally, as shown in Figure S4, a colloidal stability test analyzed by DLS demonstrates that the size does not significantly increase due to further aggregation in serum conditions.

Selective Drug Delivery by Apt-Nanospheres. To verify the highly drug-loaded and selective drug delivery of apt-nanospheres, we evaluated the selective transport of Dox-loaded apt-nanospheres using confocal microscopy (detailed

https://doi.org/10.1021/acsami.2c10397
ACS Appl. Mater. Interfaces XXXX, XXX, XXX−XXX

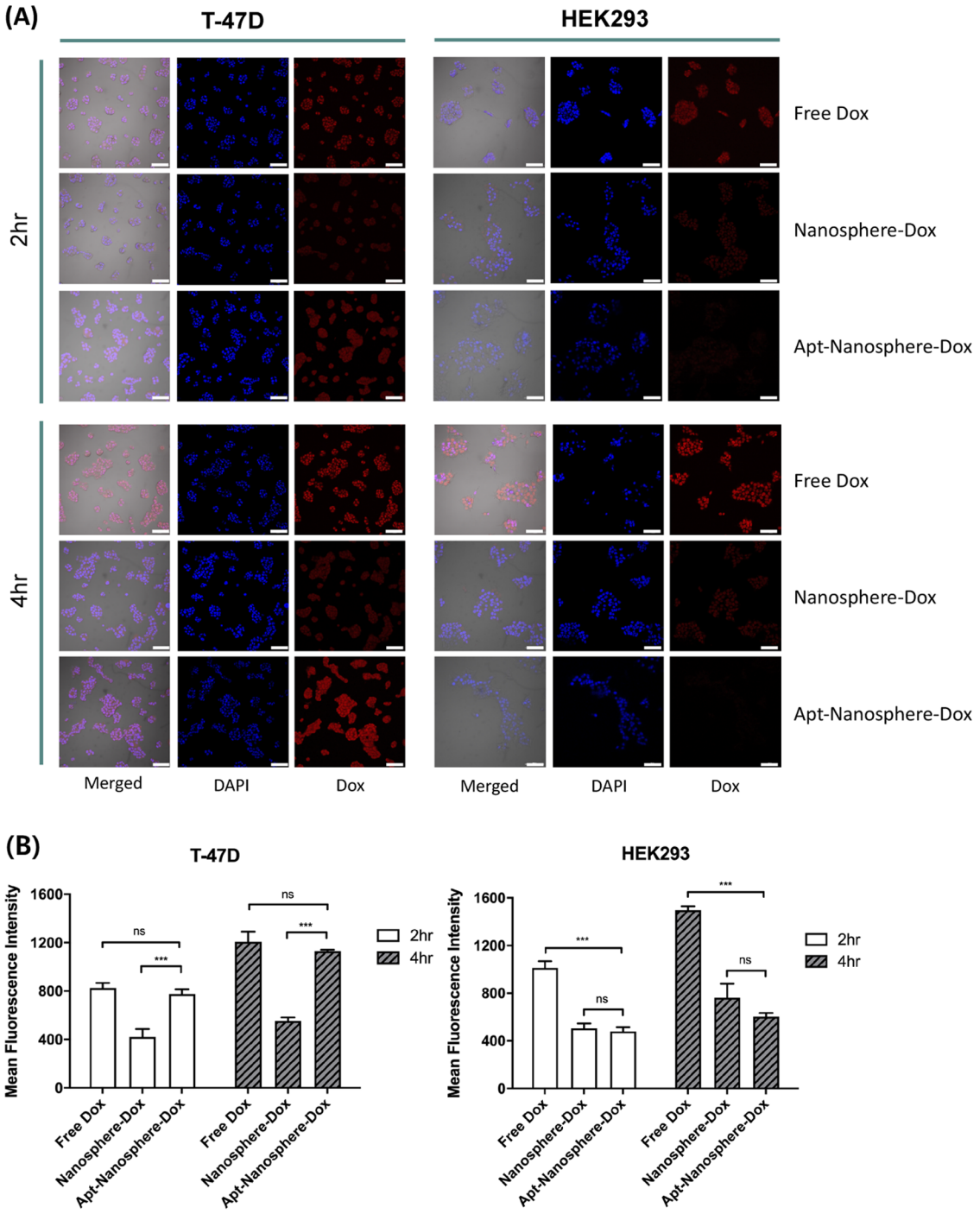

Figure 5. Fluorescence confocal laser scanning microscopy (CLSM) images of (A) T-47D and HEK293 cells after incubation with free Dox, Dox-loaded nanosphere (Nanosphere-Dox), and aptamer decorated nanospheres (Apt-Nanosphere-Dox) with different incubation times (scale bar = 100 μm). The Dox concentration was 1.5 μM. The red regions show the localization of Dox, and the blue regions show cellular nuclei (DAPI). (B, C) Dox mean fluorescence intensities (MFI) (*** indicates significance with $p < 0.001$, and ns indicates $p > 0.05$. Data expressed as the mean ± SEM, $n = 3$).

procedures in Supporting Information S11). Free Dox, Dox-loaded nanospheres, and Dox-loaded apt-nanospheres (1 μM Dox equivalents) were inoculated separately and incubated for different time durations. As shown in Figure 5, when cells were treated with free Dox, intense fluorescence doxorubicin signals were observed in those cells, whereas with Dox-loaded nanospheres, only faint signals were detected. Furthermore, we also observed signals with Dox-loaded apt-nanospheres, which we previously showed can selectively bind with MUC1 overexpressed T-47D cells. Notably, monitoring aptamer-labeled nanospheres exhibited significantly stronger signals when incubated with (MUC1+) T-47D cells (Figure 5B). Interestingly however, a different result was observed when incubated with (MUC1-) HEK293 cells (Figure 5C). In addition, we confirmed that the Dox fluorescence intensity was higher after 4 h of incubation than after 2 h in both types of cells.

https://doi.org/10.1021/acsami.2c10397
ACS Appl. Mater. Interfaces XXXX, XXX, XXX−XXX

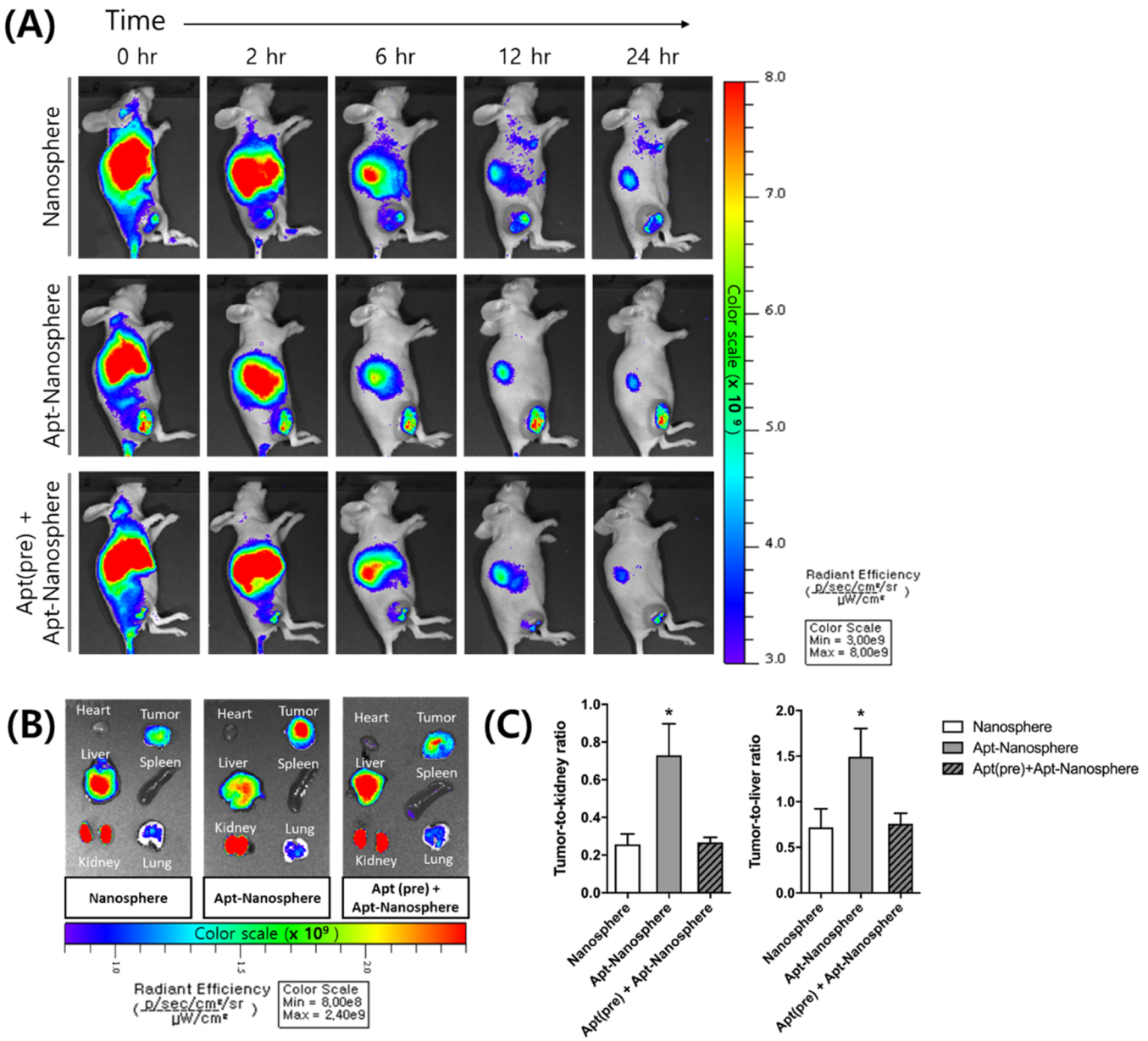

Figure 6. (A) *In vivo* and (B) *ex vivo* imaging of 4T1 tumor-bearing mice after intravenous injections of Cy5.5-labeled nanospheres, apt-nanospheres, and aptamer preinjected apt-nanospheres, and (C) *ex vivo* analysis.

***In Vitro* Cytotoxicity Assay.** Recognizing the selective Dox transportation of apt-nanospheres in Figure 5, we anticipated that because Dox kills the cells and suppresses growth, it could negatively affect cell viability. We therefore performed an *in vitro* cytotoxicity test against target T-47D cells and nontarget HEK293 cells (detailed procedures in Supporting Information S12). According to Figure S10, the nanospheres without Dox-loading did not show signs of cytotoxicity. However, as shown in Figure S9, target T-47D cells (A) and nontarget HEK293 cells (B) were each incubated with Dox-nanospheres and Dox-apt-nanospheres separately and tested using CCK-8. Dox-loaded aptamer-modified nanospheres exhibited selectivity specifically for T-47D cells (Figure S9A). This implies the potential capability of apt-nanospheres for targeted delivery.

***In Vivo* Biocompatibility Assessment of Apt-Nanospheres.** The injection of biomaterials is known to cause cascades of reactions in *in vivo* environments. Therefore, prior to use as a drug delivery carrier, it is necessary to demonstrate biocompatibility by evaluating the *in vivo* toxicity. We intravenously administered apt-nanospheres and saline to BALB/c nude mice to assess the toxicity of apt-nanospheres compared to saline. Fourteen days after the injection, blood samples were collected to evaluate the effects on the liver and kidneys.[49] Aspartate aminotransferase (AST), alanine transaminase (ALT), blood urea nitrogen (BUN), and creatinine levels were measured as shown in Figure S11. After collecting blood from the mice, we harvested the major organs and obtained histopathological images as shown in Figure S12. When comparing the group administered with apt-nanospheres and the group administered with saline, the apt-nanosphere group was more similar to the control group.

***In Vivo* and *Ex Vivo* Fluorescence Imaging for Tumor Targeting Efficiency.** To demonstrate biodistribution, *in vivo* fluorescence images were acquired 0, 2, 4, 6, 12, and 24 h after treatment using the IVIS Lumina X5 Imaging System

https://doi.org/10.1021/acsami.2c10397
ACS Appl. Mater. Interfaces XXXX, XXX, XXX−XXX

(PerkinElmer). In this experiment, we injected 4T1 cells into BALB/c nude mice instead of the well-known MUC1 overexpressed cell line, T-47D. 4T1 shows a low MUC1 expression level in Figure S7, but the cell line mimics the human breast cancer model when inoculated into BALB/c mice and proliferates rapidly, making it easier to make tumor-bearing animal models. Using the IVIS bioimaging system, we analyzed the biodistribution of nanoparticles after administration to determine if they selectively bind to tumors and enter them actively or passively *in vivo*.[50] BALB/c nude mice were divided into three groups according to the administration of nanoparticles: saline (three mice), Cy5.5-labeled apt-nanospheres (three mice), and excessive aptamer preinjected Cy5.5-labeled apt-nanospheres (three mice) (detailed procedures in Supporting Information S15). As seen in Figure 6A, plain nanospheres show passive delivery to tumors according to the enhanced permeability and retention (EPR) effect.[51] Furthermore, active targeting of apt-nanospheres confirmed that the injection of apt-nanosphere more selectively penetrates into the tumor than in the group injected with only nanospheres.[52] The active targeting of cancer cells can also be demonstrated by decreasing the fluorescence intensity when MUC1 proteins are blocked by pretreated aptamers. This behavior can be demonstrated if the effect of apt-nanospheres is due to the aptamer ligand's active targeting effect. To calculate the tumor-to-organ ratio, *ex vivo* fluorescence imaging was conducted on the tumor and major organs such as the heart, liver, kidneys, spleen, and lungs (Figure 6B). We confirmed that apt-nanospheres mainly accumulated in the kidney, as proved in other DNA-based nano-drug-carrier references.[53] We also calculated the tumor-to-kidney and tumor-to-liver ratios and then confirmed that apt-nanospheres accumulated in the tumor significantly more than nanospheres did (Figure 6C).

Statistical Analysis. Statistical analysis was performed using GraphPad Prism 9. One-way or Two-way analysis of variance (ANOVA) was applied for multiple comparisons of means using Tukey's test. *, **, ***, **** indicate values of $p < 0.05$, $p < 0.01$, $p < 0.001$ and $p < 0.0001$, respectively, that were considered significant. The data were shown as mean ± 1 SEM.

CONCLUSIONS

Doxorubicin is a well-known drug in chemotherapeutics due to its broad-spectrum antitumor effect against various cancers, including solid and hematological malignancies.[54] However, doxorubicin alone has difficulties accruing at high enough in-tumor concentrations to kill cancer cells. Conversely, it is also an insufficient treatment due to its toxicity toward normal cells. As a part of efforts to overcome the nonspecific distribution of Dox, targeted therapy using nanoparticle carriers has been introduced as a potential solution.[55] Most nanoparticles used in drug delivery systems have unique biological properties that allow them to penetrate deep into tumor tissues and deliver anticancer drugs with high efficiency. Nevertheless, only a few materials have been available for drug delivery due to problems of systemic toxicity. Herein, we demonstrated a biocompatible drug delivery carrier made of DNA and protein, synthesized by a one-pot self-assembly system with a stepwise reaction mechanism. The synthesis process through self-assembly was carried out in three steps: step-growth polymerization, streptavidin−biotin conjugation, and aptamer decoration. This manuscript detailed many advantages of self-assembled DNA−protein hybrid nanospheres: biocompatibility, high drug payload capacity, biodegradability, stability, *in vivo* imaging ability, and *in vitro*/*vivo* cancer targeting ability. These characteristics have been found to be effective for tumor treatment without adverse side effects.[34] While in this study, we selected the MUC1 target aptamer (MA3) to attach to nanospheres, in future studies, we can utilize different aptamers able to bind to other cancer-specific markers, according to tumor heterogeneity. Furthermore, in addition to aptamers, nanomaterials with other functional moieties (e.g., metallic nanoparticles, peptides, polymers) can easily decorate nanospheres wherever biotin is attached, thus leading to more advanced carriers for targeted cancer treatments. This nanosphere platform can hence be applied to a wide range of therapeutic areas and has the potential to become a highly efficient and versatile nano-drug-carrier for advanced targeted cancer therapy.

EXPERIMENTAL SECTION

For detailed information of materials and experimental procedures of nanosphere synthesis, characterization, and the analysis method, refer to the Supporting Information.

ASSOCIATED CONTENT

Supporting Information

The Supporting Information is available free of charge at https://pubs.acs.org/doi/10.1021/acsami.2c10397.

Experimental details, materials and methods, and additional characterization data include morphology of dsDNA and streptavidin hybrid nanostructures with different ratios; fluorescence image of FAM-tagged nanospheres; ζ-potential measurements; stability of the nanosphere and dsDNA in denaturing agents; colloidal stability test of nanospheres in PBS and DMEM; fluorescence intensity−concentration curve of Dox in PBS; MUC1 western blotting results; flow cytometry with different variations of aptamer ratio to the nanosphere; *in vitro* cytotoxicity of Dox-loaded apt-nanospheres, and nanospheres; blood serum test; and hematoxylin−eosin (H&E)-stained images (PDF)

AUTHOR INFORMATION

Corresponding Authors

Hyung-Jun Im − *Department of Applied Bioengineering, Graduate School of Convergence Science and Technology, Seoul National University, Seoul 08826, Republic of Korea; Department of Molecular Medicine and Biopharmaceutical Sciences, Graduate School of Convergence Science and Technology, Seoul National University, Seoul 08826, Republic of Korea; Cancer Research Institute, Seoul National University, Seoul 03080, Republic of Korea; Research Institute for Convergence Science, Seoul National University, Seoul 08826, Republic of Korea;* orcid.org/0000-0002-4368-6685; Email: iihjjj@snu.ac.kr

Yoon-Kyu Song − *Department of Applied Bioengineering, Graduate School of Convergence Science and Technology, Seoul National University, Seoul 08826, Republic of Korea; Advanced Institutes of Convergence Technology, Suwon-si, Gyeonggi-do 16229, Republic of Korea; Research Institute for Convergence Science, Seoul National University, Seoul 08826, Republic of Korea;* orcid.org/0000-0002-0558-6368; Email: songyk@snu.ac.kr

https://doi.org/10.1021/acsami.2c10397
ACS Appl. Mater. Interfaces XXXX, XXX, XXX−XXX

Authors

Dayoung Lee − *Department of Applied Bioengineering, Graduate School of Convergence Science and Technology, Seoul National University, Seoul 08826, Republic of Korea; Department of Chemical Engineering, Columbia University, New York, New York 10027, United States;* orcid.org/0000-0002-3956-0203

Seungki Baek − *Department of Applied Bioengineering, Graduate School of Convergence Science and Technology, Seoul National University, Seoul 08826, Republic of Korea*

Young-Youb Kim − *Department of Applied Bioengineering, Graduate School of Convergence Science and Technology, Seoul National University, Seoul 08826, Republic of Korea*

Yongbin Bang − *Department of Applied Bioengineering, Graduate School of Convergence Science and Technology, Seoul National University, Seoul 08826, Republic of Korea; Advanced Institutes of Convergence Technology, Suwon-si, Gyeonggi-do 16229, Republic of Korea;* orcid.org/0000-0002-7296-7814

Han Na Jung − *Department of Applied Bioengineering, Graduate School of Convergence Science and Technology, Seoul National University, Seoul 08826, Republic of Korea*

Complete contact information is available at: https://pubs.acs.org/10.1021/acsami.2c10397

Author Contributions

[⊥]D.L. and S.B. contributed equally to this work. Y.-K.S., H.-J.I., and D.L. designed the project. D.L. and S.B. synthesized the nanocarriers and tested their characteristics. Y.B. and H.N.J. participated in the cell experiments and D.L. tested all assessments *in vitro*. D.L. and S.B. tested all assessments *in vivo*. D.L., Y.-Y.K., and S.B. analyzed experimental results. All authors discussed the results. D.L, S.B., H.-J.I., and Y.-K.S. wrote the manuscript with input from all authors. All authors have given approval to the final version of the manuscript.

Funding

This research was supported by the National Research Foundation (NRF) grant funded by the Korean government (MSIT) (Y.-K.S.: NRF-2020R1A2C101495311, H.-J.I.: NRF-2021M2E8A1039564).

Notes

The authors declare no competing financial interest.

REFERENCES

(1) van der Meel, R.; Sulheim, E.; Shi, Y.; Kiessling, F.; Mulder, W. J. M.; Lammers, T. Smart cancer nanomedicine. *Nat. Nanotechnol.* **2019**, *14*, 1007−1017.

(2) Shi, J. J.; Kantoff, P. W.; Wooster, R.; Farokhzad, O. C. Cancer nanomedicine: progress, challenges and opportunities. *Nat. Rev. Cancer* **2017**, *17*, 20−37.

(3) Hartshorn, C. M.; Bradbury, M. S.; Lanza, G. M.; Nel, A. E.; Rao, J. H.; Wang, A. Z.; Wiesner, U. B.; Yang, L.; Grodzinski, P. Nanotechnology Strategies To Advance Outcomes in Clinical Cancer Care. *ACS Nano* **2018**, *12*, 24−43.

(4) Farokhzad, O. C.; Langer, R. Impact of Nanotechnology on Drug Delivery. *ACS Nano* **2009**, *3*, 16−20.

(5) Tibbitt, M. W.; Dahlman, J. E.; Langer, R. Emerging Frontiers in Drug Delivery. *J. Am. Chem. Soc.* **2016**, *138*, 704−717.

(6) Chen, H. M.; Zhang, W. Z.; Zhu, G. Z.; Xie, J.; Chen, X. Y. Rethinking cancer nanotheranostics. *Nat. Rev. Mater.* **2017**, *2*, No. 17024.

(7) Li, Z. F.; Di, C. Z.; Li, S. P.; Yang, X. L.; Nie, G. J. Smart Nanotherapeutic Targeting of Tumor Vasculature. *Acc. Chem. Res.* **2019**, *52*, 2703−2712.

(8) Wilhelm, S.; Tavares, A. J.; Dai, Q.; Ohta, S.; Audet, J.; Dvorak, H. F.; Chan, W. C. W. Analysis of nanoparticle delivery to tumours. *Nat. Rev. Mater.* **2016**, *1*, No. 16014.

(9) Han, Y. S.; Shchukin, D.; Yang, J.; Simon, C. R.; Fuchs, H.; Mohwald, H. Biocompatible Protein Nanocontainers for Controlled Drugs Release. *ACS Nano* **2010**, *4*, 2838−2844.

(10) Pearce, A. K.; Simpson, J. D.; Fletcher, N. L.; Houston, Z. H.; Fuchs, A. V.; Russell, P. J.; Whittaker, A. K.; Thurecht, K. J. Localised delivery of doxorubicin to prostate cancer cells through a PSMA-targeted hyperbranched polymer theranostic. *Biomaterials* **2017**, *141*, 330−339.

(11) Liu, Q.; Zhan, C. Y.; Kohane, D. S. Phototriggered Drug Delivery Using Inorganic Nanomaterials. *Bioconjugate Chem.* **2017**, *28*, 98−104.

(12) Kono, K.; Takashima, M.; Yuba, E.; Harada, A.; Hiramatsu, Y.; Kitagawa, H.; Otani, T.; Maruyama, K.; Aoshima, S. Multifunctional liposomes having target specificity, temperature-triggered release, and near-infrared fluorescence imaging for tumor-specific chemotherapy. *J. Controlled Release* **2015**, *216*, 69−77.

(13) Li, J. Y.; Mooney, D. J. Designing hydrogels for controlled drug delivery. *Nat. Rev. Mater.* **2016**, *1*, No. 16071.

(14) Daly, A. C.; Riley, L.; Segura, T.; Burdick, J. A. Hydrogel microparticles for biomedical applications. *Nat. Rev. Mater.* **2020**, *5*, 20−43.

(15) Criscione, J. M.; Le, B. L.; Stern, E.; Brennan, M.; Rahner, C.; Papademetris, X.; Fahmy, T. M. Self-assembly of pH-responsive fluorinated dendrimer-based particulates for drug delivery and noninvasive imaging. *Biomaterials* **2009**, *30*, 3946−3955.

(16) Brown, T. D.; Whitehead, K. A.; Mitragotri, S. Materials for oral delivery of proteins and peptides. *Nat. Rev. Mater.* **2020**, *5*, 127−148.

(17) Jiang, D.; England, C. G.; Cai, W. DNA nanomaterials for preclinical imaging and drug delivery. *J. Controlled Release* **2016**, *239*, 27−38.

(18) Hu, Q. Q.; Li, H.; Wang, L. H.; Gu, H. Z.; Fan, C. H. DNA Nanotechnology-Enabled Drug Delivery Systems. *Chem. Rev.* **2019**, *119*, 6459−6506.

(19) Roberts, T. C.; Langer, R.; Wood, M. J. A. Advances in oligonucleotide drug delivery. *Nat. Rev. Drug Discovery* **2020**, *19*, 673−694.

(20) Oh, J. Y.; Kim, H. S.; Palanikumar, L.; Go, E. M.; Jana, B.; Park, S. A.; Kim, H. Y.; Kim, K.; Seo, J. K.; Kwak, S. K.; Kim, C.; Kang, S.; Ryu, J. H. Cloaking nanoparticles with protein corona shield for targeted drug delivery. *Nat. Commun.* **2018**, *9*, No. 4548.

(21) Zhou, K.; Dong, J. Y.; Zhou, Y. H.; Dong, J. C.; Wang, M.; Wang, Q. B. Toward Precise Manipulation of DNA-Protein Hybrid Nanoarchitectures. *Small* **2019**, *15*, 1804044.

(22) Praetorius, F.; Dietz, H. Self-assembly of genetically encoded DNA-protein hybrid nanoscale shapes. *Science* **2017**, *355*, No. eaam5488.

(23) Lin, Z. W.; Emamy, H.; Minevich, B.; Xiong, Y.; Xiang, S. T.; Kumar, S.; Ke, Y. G.; Gang, O. Engineering Organization of DNA Nano-Chambers through Dimensionally Controlled and Multi-Sequence Encoded Differentiated Bonds. *J. Am. Chem. Soc.* **2020**, *142*, 17531−17542.

(24) Macfarlane, R. J.; Lee, B.; Jones, M. R.; Harris, N.; Schatz, G. C.; Mirkin, C. A. Nanoparticle Superlattice Engineering with DNA. *Science* **2011**, *334*, 204−208.

(25) Li, M. H.; Luo, Z.; Zhao, Y. L. Self-Assembled Hybrid Nanostructures: Versatile Multifunctional Nanoplatforms for Cancer Diagnosis and Therapy. *Chem. Mater.* **2018**, *30*, 25−53.

(26) Kim, Y. Y.; Bang, Y.; Lee, D.; Kang, M.; Song, Y. K. Step-growth polymerization of traptavidin-DNA conjugates for plasmonic nanostructures. *Chin. Chem. Lett.* **2020**, *31*, 1137−1140.

(27) Wan, L.; Chen, Q. S.; Liu, J. B.; Yang, X. H.; Huang, J.; Li, L.; Guo, X.; Zhang, J.; Wang, K. M. Programmable Self-Assembly of DNA-Protein Hybrid Hydrogel for Enzyme Encapsulation with Enhanced Biological Stability. *Biomacromolecules* **2016**, *17*, 1543−1550.

(28) Kim, Y. Y.; Bang, Y.; Lee, A. H.; Song, Y. K. Multivalent Traptavidin-DNA Conjugates for the Programmable Assembly of Nanostructures. *ACS Nano* **2019**, *13*, 1183−1194.
(29) McMillan, J. R.; Hayes, O. G.; Remis, J. P.; Mirkin, C. A. Programming Protein Polymerization with DNA. *J. Am. Chem. Soc.* **2018**, *140*, 15950−15956.
(30) So, Y. H. The effect of limited monomer solubility in heterogeneous step-growth polymerization. *Acc. Chem. Res.* **2001**, *34*, 753−758.
(31) Lu, X. G.; Fu, H. L.; Shih, K. C.; Jia, F.; Sun, Y. H.; Wang, D. L.; Wang, Y. Y.; Ekatan, S.; Nieh, M. P.; Lin, Y.; Zhang, K. DNA-Mediated Step-Growth Polymerization of Bottlebrush Macromonomers. *J. Am. Chem. Soc.* **2020**, *142*, 10297−10301.
(32) Lao, Y. H.; Phua, K. K. L.; Leong, K. W. Aptamer Nanomedicine for Cancer Therapeutics: Barriers and Potential for Translation. *ACS Nano* **2015**, *9*, 2235−2254.
(33) Meng, H. M.; Liu, H.; Kuai, H. L.; Peng, R. Z.; Mo, L. T.; Zhang, X. B. Aptamer-integrated DNA nanostructures for biosensing, bioimaging and cancer therapy. *Chem. Soc. Rev.* **2016**, *45*, 2583−2602.
(34) Baldus, S. E.; Wienand, J. R.; Werner, J. P.; Landsberg, S.; Drebber, U.; Hanisch, F. G.; Dienes, H. P. Expression of MUC1, MUC2 and oligosaccharide epitopes in breast cancer: Prognostic significance of a sialylated MUC1 epitope. *Int. J. Oncol.* **2005**, *27*, 1289−1297.
(35) Hu, Y.; Duan, J.; Zhan, Q.; Wang, F.; Lu, X.; Yang, X. D. Novel MUC1 aptamer selectively delivers cytotoxic agent to cancer cells in vitro. *PLoS One* **2012**, *7*, No. e31970.
(36) Walsh, M. D.; Luckie, S. M.; Cummings, M. C.; Antalis, T. M.; McGuckin, M. A. Heterogeneity of MUC1 expression by human breast carcinoma cell lines in vivo and in vitro. *Breast Cancer Res. Treat.* **1999**, *58*, 253−264.
(37) Solatycka, A.; Owczarek, T.; Piller, F.; Piller, V.; Pula, B.; Wojciech, L.; Podhorska-Okolow, M.; Dziegiel, P.; Ugorski, M. MUC1 in human and murine mammary carcinoma cells decreases the expression of core 2 beta 1,6-N-acetylglucosaminyltransferase and beta-galactoside alpha 2,3-sialyltransferase. *Glycobiology* **2012**, *22*, 1042−1054.
(38) Mahanta, S.; Fessler, S. P.; Park, J.; Bamdad, C. A Minimal Fragment of MUC1 Mediates Growth of Cancer Cells. *PLoS One* **2008**, *3*, No. e2054.
(39) Chen, W. L.; Li, F.; Tang, Y.; Yang, S. D.; Li, J. Z.; Yuan, Z. Q.; Liu, Y.; Zhou, X. F.; Liu, C.; Zhang, X. N. Stepwise pH-responsive nanoparticles for enhanced cellular uptake and on-demand intracellular release of doxorubicin. *Int. J. Nanomed.* **2017**, *Volume 12*, 4241−4256.
(40) de Lázaro, I.; Mooney, D. J. A nanoparticle's pathway into tumours. *Nat. Mater.* **2020**, *19*, 486−487.
(41) Poon, W.; Kingston, B. R.; Ouyang, B.; Ngo, W.; Chan, W. C. W. A framework for designing delivery systems. *Nat. Nanotechnol.* **2020**, *15*, 819−829.
(42) Wan, L. Y.; Yuan, W. F.; Ai, W. B.; Ai, Y. W.; Wang, J. J.; Chu, L. Y.; Zhang, Y. Q.; Wu, J. F. An exploration of aptamer internalization mechanisms and their applications in drug delivery. *Expert Opin. Drug Delivery* **2019**, *16*, 207−218.
(43) Pérez-Arnaiz, C.; Busto, N.; Leal, J. M.; Garcia, B. New Insights into the Mechanism of the DNA/Doxorubicin Interaction. *J. Phys. Chem. B* **2014**, *118*, 1288−1295.
(44) Kim, I.; Byeon, H. J.; Kim, T. H.; Lee, E. S.; Oh, K. T.; Shin, B. S.; Lee, K. C.; Youn, Y. S. Doxorubicin-loaded highly porous large PLGA microparticles as a sustained-release inhalation system for the treatment of metastatic lung cancer. *Biomaterials* **2012**, *33*, 5574−5583.
(45) Jin, Y. S.; Yue, X. L.; Zhang, Q. Y.; Wu, X. Y.; Cao, Z.; Dai, Z. F. Cerasomal doxorubicin with long-term storage stability and controllable sustained release. *Acta Biomater.* **2012**, *8*, 3372−3380.
(46) Zhao, H. R.; Yuan, X. X.; Yu, J. T.; Huang, Y. S.; Shao, C.; Xiao, F.; Lin, L.; Li, Y.; Tian, L. L. Magnesium-Stabilized Multifunctional DNA Nanoparticles for Tumor-Targeted and pH-Responsive Drug Delivery. *ACS Appl. Mater. Interfaces* **2018**, *10*, 15418−15427.
(47) Li, H.; Zhou, X.; Yao, D. B.; Liang, H. J. pH-Responsive spherical nucleic acid for intracellular lysosome imaging and an effective drug delivery system. *Chem. Commun.* **2018**, *54*, 3520−3523.
(48) Chandrasekaran, A. R. Nuclease resistance of DNA nanostructures. *Nat. Rev. Chem.* **2021**, *5*, 225−239.
(49) Lee, W.; Jeon, M.; Choi, J.; Oh, C.; Kim, G.; Jung, S.; Kim, C.; Ye, S. J.; Im, H. J. Europium-Diethylenetriaminepentaacetic Acid Loaded Radioluminescence Liposome Nanoplatform for Effective Radioisotope-Mediated Photodynamic Therapy. *ACS Nano* **2020**, *14*, 13004−13015.
(50) Stewart, M. P.; Sharei, A.; Ding, X. Y.; Sahay, G.; Langer, R.; Jensen, K. F. In vitro and ex vivo strategies for intracellular delivery. *Nature* **2016**, *538*, 183−192.
(51) Rosenblum, D.; Joshi, N.; Tao, W.; Karp, J. M.; Peer, D. Progress and challenges towards targeted delivery of cancer therapeutics. *Nat. Commun.* **2018**, *9*, No. 1410.
(52) Wang, D.; Peng, R. Z.; Peng, Y. B.; Deng, Z. Y.; Xu, F. Y.; Su, Y. Y.; Wang, P. F.; Li, L.; Wang, X. Q.; Ke, Y. G.; Tan, W. H. Hierarchical Fabrication of DNA Wireframe Nanoarchitectures for Efficient Cancer Imaging and Targeted Therapy. *ACS Nano* **2020**, *14*, 17365−17375.
(53) Jiang, D. W.; Ge, Z. L.; Im, H. J.; England, C. G.; Ni, D. L.; Hou, J. J.; Zhang, L. H.; Kutyreff, C. J.; Yan, Y. J.; Liu, Y.; Cho, S. Y.; Engle, J. W.; Shi, J. Y.; Huang, P.; Fan, C. H.; Yan, H.; Cai, W. B. DNA origami nanostructures can exhibit preferential renal uptake and alleviate acute kidney injury. *Nat. Biomed. Eng.* **2018**, *2*, 865−877.
(54) Speth, P. A. J.; Vanhoesel, Q. G. C. M.; Haanen, C. Clinical Pharmacokinetics of Doxorubicin. *Clin. Pharmacokinet.* **1988**, *15*, 15−31.
(55) Li, N.; Wang, X.-Y.; Xiang, M.-H.; Liu, J.-W.; Yu, R.-Q.; Jiang, J.-H. Programmable Self-Assembly of Protein-Scaffolded DNA Nanohydrogels for Tumor-Targeted Imaging and Therapy. *Anal. Chem.* **2019**, *91*, 2610−2614.

https://doi.org/10.1021/acsami.2c10397
ACS Appl. Mater. Interfaces XXXX, XXX, XXX−XXX